









Research article

Four-dimensional printing of acrylonitrile butadiene styrene – thermoplastic polyurethane shape memory polymers with excellent material and interfacial adhesion performance

Kianoosh Soltanmohammadi¹, Mohammad Aberoumand¹, Davood Rahmatabadi¹,
Elyas Soleyman¹, Sogol Ghasemi², Ismaeil Ghasemi^{3*}, Majid Baniassadi¹,
Karen Abrinia¹, Mahdi Bodaghi⁴, Mostafa Baghani¹

¹School of Mechanical Engineering, College of Engineering, University of Tehran, Tehran, Iran

²Department of Polymer Engineering and Color Technology, Amirkabir University of Technology, Tehran, Iran

³Faculty of Processing, Iran Polymer and Petrochemical Institute, Tehran, Iran

⁴Department of Engineering, School of Science and Technology, Nottingham Trent University, Nottingham NG11 8NS, UK

Received 11 February 2023; accepted in revised form 11 July 2023

Abstract. There are a limited number of thermoplastics with intrinsic shape memory effect (SME) that are four-dimensional (4D) printable. Development of other shape memory polymers (SMPs) entails synthesis with a complicated chemical experimental lab effort. In this paper, for the first time, a novel layered multi-material structure is developed based on a deep comprehension of SMEs' macromolecular requisites. The fused deposition modeling (FDM) method is used for the four-dimensional printing of layered structures whose base materials show no SME. Commercial acrylonitrile butadiene styrene (ABS), toughened ABS-thermoplastic polyurethane (TPU) blend, and TPU, all with no SME, are used to fabricate bi-layers of ABS-TPU blends and TPU with different volumetric proportions. Different thermo-mechanical tests, including dynamic mechanical thermal analysis (DMTA), and constrained and free shape recovery, are conducted. Also, the interfacial properties of the layered 4D printed structure are assessed by the mean of shear testing and scanning electron microscopy (SEM). Experimental results reveal that the 4D printed bi-layer composites possess a high level of programmability, SME (90–96%), and perfect interfaces without any porosity and detachment between layers. The results of this research can potentially eliminate the desperate need for SMPs for 4D printing and broaden the opportunity to have smart parts using commercial thermoplastics.

Keywords: smart polymers, 4D printing, bi-layer structure, material testing, adhesion

1. Introduction

Additive manufacturing (AM) or three-dimensional (3D) printing is an emerging approach for fabricating prototypes or final parts with sophisticated geometries which cannot be produced by traditional manufacturing methods [1, 2]. This manufacturing technology has diverse usages in academics and distinctive fields of industry such as automotive, aerospace, soft robotics, fashion, and health care. The basic idea of 3D printing is the creation of a two-dimensional layer with a simple geometry on another layer to produce

a complex solid object [3, 4]. Fused deposition modeling (FDM) is the easiest, most controllable, and most efficient technique of AM to manufacture thermoplastic parts. Furthermore, because of the low cost of base materials in this technique, it is surprisingly economical [5]. The fundamental concept of its procedure is the extrusion of semi-liquid thermoplastic. In the last decade, there have been many prominent experimental and numerical investigations on the FDM technique related to improving the material properties of 3D printed parts [6] and multi-material

*Corresponding author, e-mail: i.ghasemi@ippi.ac.ir

© BME-PT

and gradient printing [7–9]. Multi-material FDM printing is related to printing different filaments by dual extruder printers [7, 9–11] or using continuous fibers embedded in filaments and printing them with an especially designed extruder [12, 13]. Of course, the manufacturing of composite shape memory polymers (SMPs) has also been developed to achieve non-thermal stimulation, such as electrical [14]. Shape memory materials (SMMs) are a kind of smart materials that have captivated industries and academic researchers for the last couple of decades. These materials' shapes can be converted in response to a specific stimulus [15]. The most important characteristic of the SMMs is the shape memory effect (SME), in which the original shape is 'memorized' and recovered freely without any additional mechanical force [16, 17]. SMPs are the most well-known types of SMMs due to their unique properties. Some of their features and advantages are: fixing and recovering large strains, high recovery rate, tailorable properties (e.g., transition temperature), programmability and controllability of recovery, low cost, lightweight, acquiring potential of biodegradability and biocompatibility, and vast types of stimuli including joule heating, electrical current, magnetic field, light exposure, UV exposure, moisture, pH and mechanical loading, etc. [18–20]. For manifestation SME, polymers must have net points or hard phase and soft phase. The hard phase is needed to form an integrated polymeric network that stores the strain energy and releases it in the recovery step for memorization of the permanent shape. These net points can be chemical crosslinks for thermosets and crystalline or molecular entanglements as physical crosslinks for thermoplastic polymers. The responsibility of fixing the temporary shape after the programming steps and recovering the applied deformation is due to the soft phase [21, 22]. Four-dimensional (4D) printing is a scientific horizon that is the integration of two concepts of AM and the capability to change the shape like an SME [23]. The dynamic properties of 4D-printed SMMs are related to the fourth dimension of printing. FDM is the most used technique in 4D printing [24, 25]. Nevertheless, only a few thermoplastic SMPs like polylactic acid (PLA) and polyurethane (PU) are 4D printable, and to make novel SMPs, additional operations such as blending polymers are needed [17, 26]. In this regard, based on the multi-material printing and the microscopic concept of SMPs, a shape memory bi-layer structure is developed here.

Acrylonitrile butadiene styrene (ABS) and thermoplastic polyurethane (TPU) are commercial filaments in 3D printing that are employed in this research. In multi-material printing, the adhesion of the polymers in joint surfaces is one of the most prominent points and is generally limited to three theories, including mechanical interlocking, diffusion, and thermodynamic theory of adhesion [27–30]. There are only a few experimental and numerical investigations on the adhesion of these two materials, specifically in the AM field. Harris *et al.* [31] printed a three-layered ABS/TPU/ABS structure. The shear test results suggested that TPU adheres to ABS, which was comparable to the commercial adhesive. Another achievement of their work was that the TPU layer adheres to lower ABS better than the upper ABS layer. The reason was that at the printing temperature of TPU (218 °C), the complex viscosity of this material is much lower than ABS at its printing temperature (240 °C). This phenomenon led to excellent interlocking and filling of voids in bottom-layered ABS with TPU. In contrast, the top layer of ABS could not establish the same interlocking as TPU. Yin *et al.* [32] conducted an experimental and numerical investigation on the interfacial bonding of ABS and TPU based on the diffusion aspect of adhesion. They evaluated the effects of building stage temperature, print speed, and nozzle temperature on the quality of the interfacial bonding of the ABS and TPU printed alongside each other. They have found that by increasing the building stage temperature from 30 to 68 °C, the bonding significantly improved from 0.86 to 1.66 MPa. By decreasing the printing speed and increasing the nozzle temperature, also the bonding was enhanced, but these parameters had minor effects. They also insisted that for diffusion, both materials must be above their glass transition temperature (T_g) during the printing of each layer. de León *et al.* [27] blended the ABS and TPU with different weight percentages (the blends contained 10, 20, and 30 wt% of TPU) to study the compatibility of these materials. Fourier transform infrared (FTIR) spectroscopy analysis in attenuated total reflectance mode (ATR), atomic force microscopy (AFM) and Raman spectroscopy were carried out in the study. The results showed a homogeneous distribution of ABS and TPU in the blends, probably due to hydrogen bonding supramolecular interactions between TPU polar groups and ABS acrylonitrile and aromatic moieties. AFM phase images presented that in the

blends with 10 wt% TPU, it was homogeneously distributed within the ABS matrix, while for blends containing 30 wt% TPU, it tended to form a continuous phase along the ABS matrix. They also printed tensile test specimens with the blend to obtain mechanical properties. Due to the observations, the presence of TPU improved interlayer adhesion without deterioration of yield strength for composition up to 20 wt%.

As it is aforementioned, ABS is the common filament for FDM, and it also has perfect mechanical properties. Due to the importance of producing functional objects, for example, actuators or shock absorbers, scientists have utilized distinctive approaches [33]. One of these approaches is the printing of flexible materials [34]. Therefore, ABS, as the common material, has been toughened with different elastomers and plasticizers in different examinations [27, 34, 35]. Also, the toughening of ABS through blending with another compatible material has another functional advantage which is the reduction of its T_g [34, 36]. de León *et al.* [27] blended ABS with 30 wt% of TPU. They could triple the elongation at the breaking point without any remarkable drop in yield strength in comparison to the neat ABS. Siqueiros *et al.* [34] developed a new filament with ABS and thermoplastic elastomer styrene ethylene butylene grafted with maleic anhydride (SEBS-*g*-MA). They melted and blended these two materials with distinctive concentrations and could increase the elongation at the break values from 8.5% for neat ABS to 50% for ABS/SEBS-*g*-MA 50/50 composition.

In this article, for the first time, 4D printed shape memory bi-layer structures were developed from a non-shape memory thermoplastic (ABS) and an elastomer (TPU). The generalization of SMPs' microstructural concept to a macrostructural structure is employed to achieve the SME in these 4D printed specimens. Also, in comparison to the previous investigations of multilayer SMPs produced by co-extrusion, these 4D printed structures benefited from the 3D printing's positive points, especially for producing complex geometries for applications like pipe fasteners. To achieve high deformability, reduce the T_g and improve the adhesion between the materials, ABS was blended with TPU at two different weight percentages (80 and 60 wt%). Bi-layer ABS-TPU structures were printed with different layer thicknesses of components, and SME (shape fixity, shape

recovery, and stress recovery) was investigated through constrained and free stress recovery. Additionally, a dynamic mechanical thermal analysis (DMTA), a shear test, and scanning electron microscopy (SEM) were conducted to scrutinize the thermal behavior and adhesion between TPU and the neat ABS and blends.

2. Experimental procedures

2.1. Materials and filament preparation

Commercial ABS granules were purchased from Baspar Chemi Sepidan Co, Ltd (Iran). Also, polyester-based TPU granules with the grade of 365A were prepared from Xiamen Keyuan Plastic Co., Ltd (China) to be used for ABS/TPU blends. A black-colored filament of TPU was obtained from Shenzhen Esun Industrial Co., Ltd. (China) that is printed as the elastomeric layer. Before starting any process, all of the materials were dried for 3 h at 80 °C. Different ABS-TPU blends were mixed by varying weight percentages of 365A TPU: 20, and 40% (in terms of ABS80, ABS60). The materials were blended using a Coperion twin screw extruder (Model ZSK-25, Coperion GmbH, Stuttgart, Germany) with an L/D of 40 and a screw diameter of 25 mm to produce a filament. The processing temperature window was between 200 to 220 °C with a screw speed of 70 rpm. The filament was cut into palettes. Then, neat ABS, ABS80, and ABS60 blend palettes were used to prepare FDM filaments with 1.75 mm diameter by a lab-made single screw extruder with an L/D of 15 and screw diameter of 15 mm with a speed and temperature of 30 rpm and 230 °C, respectively.

2.2. Printing procedure

A desktop two-nozzle FDM printer with a 0.8 mm nozzle diameter was employed to print all samples. The infill density of parts was 100% with a raster angle of 0° and layer thickness of 200 μm. For all bi-layer samples, the black-colored TPU was printed above the neat ABS and toughened ABS blend according to Harris *et al.* [31] investigations. Regarding Yin *et al.* [32] and de León *et al.* [27] experiments, the bed temperature was chosen to be 65 °C and the printing temperatures for neat ABS, toughened ABS blends, and the black TPU were set to be 240, 240, and 230 °C, respectively. Also, the printing speed for neat ABS and toughened ABS blends was 50 mm/s, and for the black TPU was 15 mm/s.

2.3. Dynamic mechanical thermal analysis (DMTA)

A thermal analysis was performed on the neat ABS and the ABS-TPU blends and the black-colored TPU to observe the storage modulus and the glass-rubbery transitional behavior at different temperatures. In this respect, a cantilever beam with a geometry of 40×10×1 mm was printed based on the ASTM D4065-01 standard. The test was carried out from –100 to 140 °C with a heating rate of 5 °C/min and a constant 1 Hz frequency by a dynamic mechanical thermal analyzer (Mettler Toledo GmbH, Switzerland).

2.4. Shape memory performance

For assessment of the shape memory performance of the bi-layer structures, the free and constrained shape recovery tests were executed in bending mode using a universal testing machine with a 1 kN load cell. A programmable logic controller (PLC) was employed to manipulate the temperature, heating, and cooling rates of the tests. All the bi-layer structures were printed in the geometry of 50×10×4 mm with three different ratios of TPU layer thickness to the ABS or ABS-TPU blend layer thickness (thermoplastic layer) listed in Table 1. The samples are bi-layer structures in which the thermoplastic was printed beneath the black TPU. For the free and constrained shape recovery tests, all of the samples were printed and tested three times to ensure the accuracy and repeatability of the findings.

2.4.1. Free shape recovery test

For programming, all of the twelve specimens (nine and three for shape recovery and stress recovery)

Table 1. Sample codes considering the used thermoplastic type, the thickness ratio of layers, and the structure layout.

Sample code	TPU/thermoplastic layer thickness ratio	Thermoplastic layer type
I	1:3	ABS
II	1:1	
III	3:1	
IV	1:3	ABS80
V	1:1	
VI	3:1	
VII	1:3	ABS60
VIII	1:1	
IX	3:1	

were constrained and heated to 85 °C at an 8 °C/min rate and remain in this condition for 120 s (heating step). Then a 7 mm deflection was applied to the samples at a rate of 3 mm/min (deformation step). Without any delay, the structures were quenched to ambient temperature at a rate of 30 °C/min and fixed in this circumstance for the next 240 s (cooling step). Afterward, the specimens were unloaded, and the fixity ratio was evaluated by Equation (1) (unloading step). For the shape recovery, samples were reheated to 100 °C with a high rate of 30 °C/min (recovery step). The recovery ratios were gauged after one minute of remaining at a high temperature using Equation (2). The explained cycle is a well-known SME programming cycle:

$$\text{Shape fixity ratio [\%]} = \frac{\text{Remained deflection}}{\text{Applied deflection}} \cdot 100 \quad (1)$$

$$\text{Shape recovery ratio [\%]} = \frac{\text{Recovered deflection}}{\text{Remained deflection}} \cdot 100 \quad (2)$$

2.4.2. Constrained shape recovery test

The constrained shape recovery test was executed for two-layer structures and only in the same ratio of TPU thickness to ABS thickness (Samples II, V, VIII). The three first steps of the test were exactly the same as the free shape recovery test. Then the samples were unloaded, and after holding the condition for a few seconds, the samples were confined again without any further deformation and reheated to 90 °C at the rate of 15 °C/min to examine the recovered force.

2.5. Shear test

The shear test was performed by a universal testing machine equipped with a 1 kN load cell and a sliding shear fixture. As depicted in Figure 1, the design of the fixture consists of two different pieces. A 5 mm depth groove and hole were craved on the first and second pieces. By sliding the two pieces on each other, pure shear is applied to the samples. The shear samples were designed considering the fixture geometry. The samples consist of two cubes with the geometry of 10×10×5 mm and 8×8×5 mm (Figure 1). The three reference samples of neat ABS, ABS80, and ABS60 and the three bi-layer structures consisting of them and the TPU layer were printed.

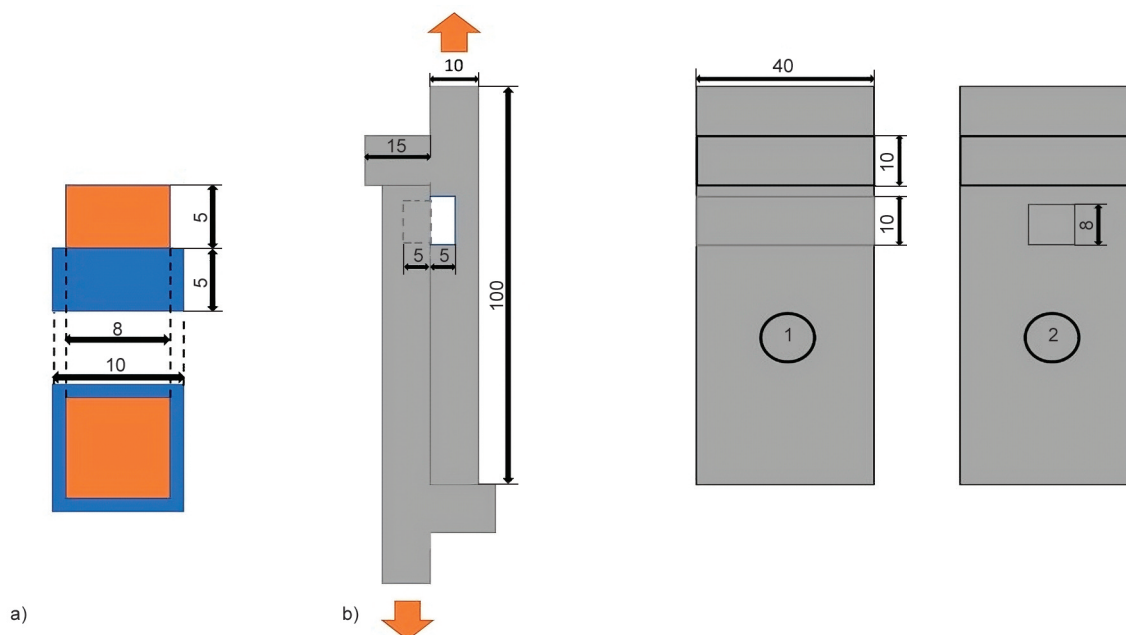


Figure 1. a) The dimensions of the shear test specimens, b) the dimensions of the sliding shear fixture, and the sliding direction (all in mm).

2.6. Scanning electron microscopy (SEM)

For the evaluation of the bond quality between the materials, imaging was also performed using SEM. Before imaging, the samples were frozen and broken down in liquid nitrogen and then coated with gold. Imaging was performed using Philips XL30 Scanning Electron Microscope (Koninklijke Philips N.V., The Netherlands) in secondary electron imaging mode.

3. Results and discussion

3.1. DMTA

The DMTA results of TPU are shown in Table 2. According to the storage modulus change, -40°C is the starting point of the glass-to-rubbery transition, and it continues until 25°C , demonstrating a wide transition range of 65°C . The $\tan \delta$ peak representing the T_g of TPU is about -1°C and its value is 0.32. Also, the storage modulus drops from 80 MPa at room temperature to 25 MPa at 85°C . This decreasing trend continues until 100°C , and the storage modulus reaches the least value of 19 MPa, which is consistent

Table 2. Storage moduli of TPU.

Quality	Temperature [°C]	Storage modulus [MPa]
Glass transition starting point	-40	2234
Glass transition ending point	25	80
Deformation point	85	25
Recovery point	100	19

with observations in [37]. The slight rise in the storage modulus of TPU during the cooling process in the shape memory cycle may slightly help the imposed strain to be stored. On the other hand, the slight increase in storage modulus upon cooling makes the TPU stiffer while it is in a rubbery state, causing the entropic force to be intensified with the same imposed strain. However, this intensified retracting force would not deteriorate the shape fixity because even the increased storage modulus of TPU at room temperature is far smaller than that of materials that possess high storage moduli in their glassy state at room temperature like ABS.

The storage modulus changes for ABS, ABS80 and ABS60 according to temperature are presented in Figure 2 and Table 3. As it is depicted in Figures 2a and 2b the glass-to-rubber transition of ABS starts from 90 to 135°C and $\tan \delta$ picks at 118°C (T_g). Also, α transition of this material occurs at 103°C , which is the middle point of the storage modulus's drop from 760 to 55 MPa. In addition, between 0 and 85°C , the storage modulus decreases from 995 to 780 MPa gradually. Also, there is a β transition for ABS between -85 and -62°C , which is consistent with observations in [37]. As aforementioned, de León *et al.* [27] reported superior compatibility between ABS and TPU, which can be distinguished in the DMTA results of ABS80 and ABS60 composites, as shown in Figures 2a and 2b. Initially, the glass transition of ABS80 and ABS60 read from 87 to

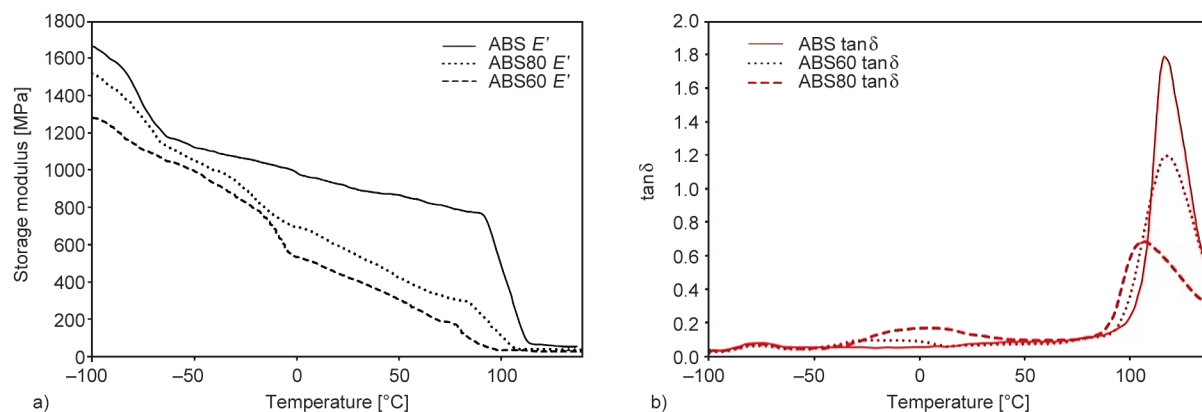


Figure 2. The results of the DMTA: a) the storage modulus, and b) $\tan \delta$ of ABS, ABS80, and ABS 60.

Table 3. The storage modulus changes according to temperature for ABS, ABS80, and ABS 60.

T [°C]	Storage modulus [MPa]		
	ABS	ABS60	ABS80
-85	1540	1400	1180
-62	1170	1110	10463
0	995	695	540
100	465	88	33
110	112	40	33
120	54	39	31

130 °C and 81 to 125 °C, respectively. Furthermore, with the increase of TPU content in the ABS matrix, the storage modulus of composite blends gets lower in the whole temperature range. Also, the reduction rate of the storage modulus in the β transition of ABS is slightly decreased for both composites. Moreover, there are additional drops from around -40 to 0 °C for both blends, especially in ABS60, which are associated with the contribution of the TPU's glass-to-rubber transition. Besides, significant continuous declining slopes in the storage modulus curves of composites are detected between 0 and 85 °C due to the corporation of TPU, which are from 695 to 270 MPa and 540 to 97 MPa for ABS80 and ABS60, respectively. Also, the glass and α transition temperatures of ABS80 are fallen to 114 and 95 °C, respectively. After surpassing the α transition temperature, the storage modulus dropped from 220 to 32 MPa. In the case of ABS60, the T_α is 87 °C, and the storage modulus decreases from 153 to 27 MPa during this transition. The T_g of this composite is 106 °C. The basic concept of the SMEs in this work, which will be discussed in the next section, is based on the storage modulus of hard material above the switching temperature, which is the α transition temperature of ABS, and both composites. Therefore, the

recovery occurs at 100 °C where the α transition is completed, and the storage moduli of ABS80 and ABS60 reach 88 and 33 MPa, respectively. This notable softening of the ABS blends at this temperature can lead to the effective release of the stress stored in the TPU layer during the recovery procedure.

3.2. Shape fixity and recovery

A comprehensive schematic representing the essential microstructural requisites for exhibiting SME is illustrated in Figure 3, separately for each programming step. The elastomeric (storing phase) and switching phase (hard material) layers in Figure 3 refer to TPU and different types of ABS, respectively. In this article, the hard phase as a network and the soft phase are generalized to a novel bi-layer macroscopic-designed SMP structure using multi-material printing and the basic microscopic concept of SMPs. These SMP structures are the assembly of a stiff non-shape memory thermoplastic with a high T_g and an elastomer with a lower T_g (below room temperature) on top of the former layer. To make a clear association between the microstructural requisites for exhibiting SME and the characteristics that belong to the proposed bi-layer, the physical state of each layer in each programming stage is shown in Figure 3. An SMP has two microstructural features that have powered it to emerge SME. First, there should be net points, forming an integrated network to restrict relative movements of the polymer chains and permanent deformations. In the designed bi-layer structure, these net points are formed from the interconnected hard phases in TPU as a thermoplastic elastomer. This feature of TPU has brought hyperelastic properties along with negligible permanent deformation. Second, there should be a phase transition for storing and relieving the applied deformation. In the bi-layer

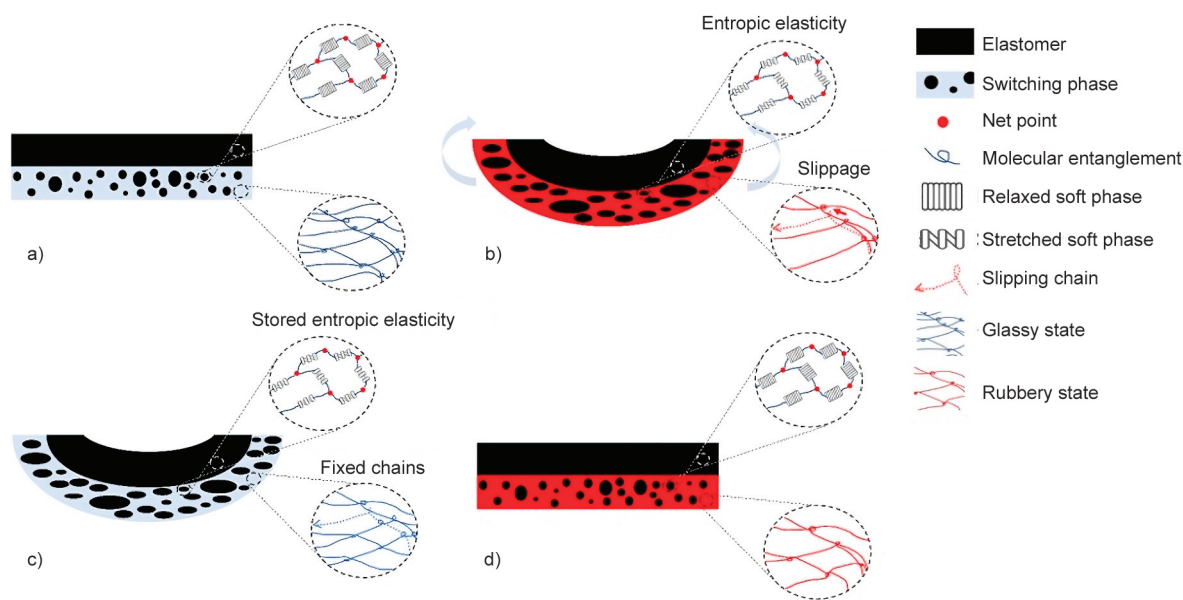


Figure 3. Schematic of samples during the shape memory cycle: a) as-printed condition, b) after heating and deformation, c) after cooling, d) recovery step.

structure, the glass transition of the polymer chains in the hard ABS layer acts similarly to an SMP. The collection of net points and phase switchable chains are found within the microstructure of an SMP. In the designed layered composite, the combination of two layers acts as a parallel spring system with the same amount of strain in each layer. The combination of the microstructural features of each layer and the parallel structural behavior can well be associated with the exact microstructural requisites that are found within an SMP. The thermoplastic is responsible for fixing the temporary shape in temperatures below T_g by the rubber-to-glass hardening transition accompanied by a substantial increase in modulus. During the programming steps, by deforming the structure, elastic stress emerges in the elastomer, and with the aid of the cooling of the deformed structure below the thermoplastic T_g , the elastic stress can be stored in the elastomer by the resists of the stiffed glassy thermoplastic. When the structure is heated above the thermoplastic T_g , the mentioned layer starts to soften, and the steep decrease in the storage modulus leads to the stored stress in the elastomer layer being released. During programming, the stress is applied to the structures, and the elastomeric layer has the duty of stabilizing most of the imposed stress thanks to the presence of an integrated network in its molecular architecture, restricting stress relaxation. Also, the thermoplastic is responsible for fixing the deflection due to its hardening behavior caused by reaching the glassy state of the material during the

cooling step (Figure 3c). The resistance of the thermoplastic layer to preserve the stored stress in the elastomeric layer (TPU) without a substantial spring back is reduced when its portion decreases. This alternation causes the structural stiffness to be lessened, which is well accompanied by a decrease in the shape fixity. In contrast, higher stress can be stored in the structure by raising the portion of the TPU layer. This phenomenon leads to a more complete shape recovery during the stimulation process (recovery step).

The shape memory performance ratios for different 4D printed bi-layer structures are named in Table 4 regarding the differences in hard material and the TPU thickness to hard material thickness ratio. All the fixed and recovered shapes of the samples are summarised in Figure 4. By comparing the samples in each set, decreasing and increasing trends are observed in shape fixity and shape recovery, respectively,

Table 4. Shape recovery and shape fixity of the samples.

Sample code	Shape fixity ratio [%]	Shape recovery ratio [%]
I	84.0	66.3
II	78.9	76.5
III	67.6	83.9
IV	94.1	87.4
V	88.6	90.5
VI	81.7	94.1
VII	89.7	93.0
VIII	86.1	94.7
IX	78.3	96.2

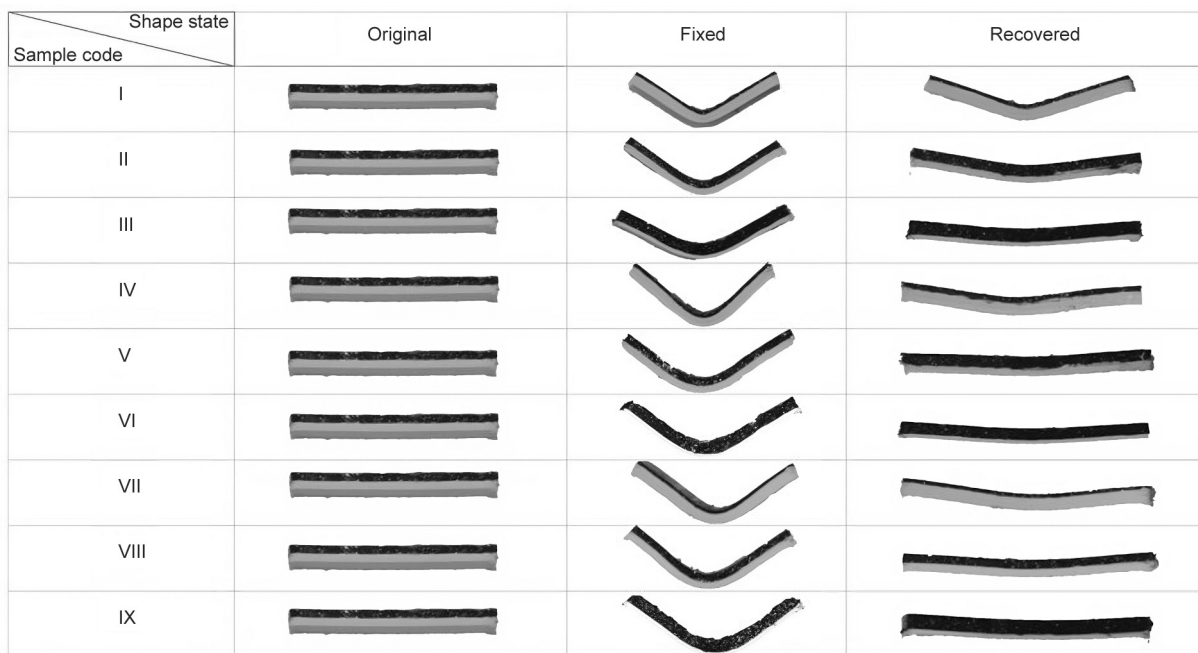


Figure 4. Fixed and recovered conditions of the coded samples.

regarding the increasing portion of the TPU layer thickness in these structures. The shape fixity ratios for the two-layer ABS-TPU structures in terms of TPU layer thickness are in the range of 67.6 to 84%, and the highest and lowest values are obtained for the highest and lowest TPU ratios, respectively. This trend is repeated for two ABS80 and ABS60 structures because increasing the layer thickness ratio of the ABS, due to its higher modulus, provides more resistance to relax the TPU layer. On the other hand, the highest amount of recovery ratio is also obtained for the lowest thickness ratio of the ABS layer because in the recovery step, the lower resistance means more recovery of the TPU elastic layer and the original shape. Shape recovery ratios are observed in the range of 66.3 and 83.9% for the two-layer structure. Shape fixity is improved in the second set compared to the first set, which is specifically related to different glass-rubber transitions of the neat ABS and ABS80. At the programming temperature (85 °C), the neat ABS structures are just at the start of their α transition, and most regions of these layers are glassy. The glassy regions can cause a more pronounced elastic and visco-elastic spring back of the structures after the unloading step at ambient temperature, which has been observed in previous sources [38]. Vice versa, the mentioned spring backs are much less in the structures with thermoplastic layers of ABS80 due to the lower temperature range of glass-to-rubber and α transitions as well as the less

portion of glassy regions in the thermoplastic layer, which contributed to the better shape fixity [39]. In the third set's samples, a drop in shape fixity compared to the second set can be observed. Less structural stiffness is achieved with the aid of the highest content of the TPU toughened into these thermoplastic layers of ABS60, which is linked to a lower shape fixity and excellent shape recovery, regardless of the thickness ratio of TPU to hard material [40].

Overall, the improving trend for shape recovery is correlated with the different glass-to-rubber regions of the neat ABS, ABS80, and ABS60 composites. As mentioned earlier, the glass-to-rubber transition is shifted to a lower range of temperatures by blending neat ABS with TPU elastomer. At 100 °C (recovery temperature), ABS60 shows the least storage moduli (33 MPa) among all three thermoplastics concerning DMTA results. This storage modulus is related to more softening of the thermoplastic composite layer at the recovery temperature, indicating weakened resistance for the release of the stored stress in the elastic layer and a resultant higher recovery ratio [40]. Also, the neat ABS and the ABS80 composites have storage moduli of 450 and 88 MPa at 100 °C, respectively, which results in a lower shape recovery ratio. From another point of view, the existence of more TPU content in the thermoplastics increases the portion of elastic material in the whole structure, which may aid in a better recovery ratio. Also, in videos 1 and 2, the programming,

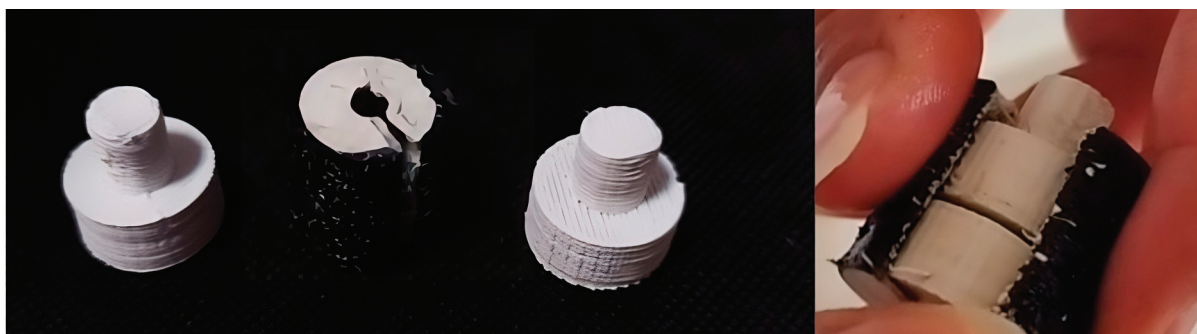


Figure 5. The customized tubular self-active bi-layer mechanical fastening.

fixity, and recovery steps of these two-layer structures can be seen.

Furthermore, a customized complex tubular self-active bi-layer structure as one of the most prominent applications of SMPs has been manufactured and presented in Figure 5. The structure is a mechanical fastening that can be used to fasten pipes [41].

3.3. Stress recovery

The stress recovery results of Samples II, V, and VIII are illustrated in Figure 6, respectively. The deformation stress of Sample II, which contains the neat ABS as the thermoplastic layer, is 10.8 MPa. Also, the maximum recovered stress for this specimen is 3.7 MPa, and it occurs at 87°C. For Sample V (ABS80 composite as a thermoplastic layer), a significant drop is observed in deformation stress which

is 5.5 MPa, and this can be related to the more softening of the ABS80 composite at the deformation temperature. This sample demonstrates a 2.45 MPa recovery stress which represents the recovery of a higher proportion of the deformation stress in comparison with the previous sample. This result is along with the earlier discussed results of the DMTA and shape memory performance that was attributed to the more softening of the thermoplastic composite layer, enabling the 4D printed bi-layer structure to recover the shape and force more intactly. The superior shape fixity of Sample V causes the TPU layer to store more of the deformation stress, and the excellent shape recovery helps this sample to recover a higher portion of the deformation stress.

Regarding DMTA results, the glass-to-rubber transition of the ABS80 composite starts at a lower

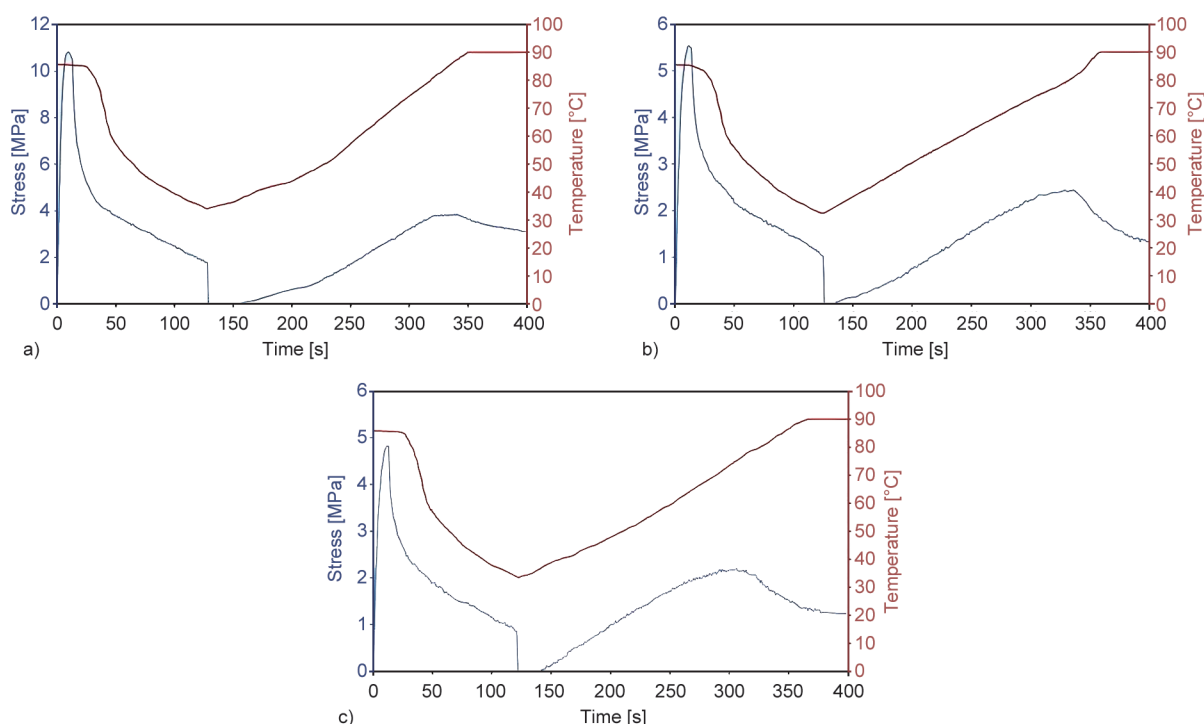


Figure 6. Stress recovery plots of the sample: a) Sample II, b) Sample V, and c) Sample VIII.

temperature. Therefore, the maximum recovery stress happens at lower temperatures of 81 °C. The last specimen's deformation stress is 4.82 MPa. This low deformation stress contributed to the smallest storage modulus of the ABS60 composite among all used thermoplastics. Furthermore, the maximum recovery stress is 2.21 MPa and occurs at 74 °C. Sample VIII is also shown a substantial stress recovery of the deformation stress, almost the same as Sample V because both samples have exhibited superior shape fixity and recovery ratios in close range to one another. By considering all of the plots, the stress in Samples V and VIII rises more sharply than the Sample II at lower temperatures. It is associated with the progressive decline of storage modulus observed in DMTA curves of the ABS80 and ABS60 composites all over the temperature range, and their lower storage modulus in each temperature leads to the release of stress progressively at lower temperatures which does not exist in the neat ABS. Moreover, by increasing the temperature, there are drops in stress after the stress recovery peaks for all samples. However, the drop for Sample II is obviously slighter than the two other specimens. This distinction is correlated to the storage modulus of the samples at 9 °C and the higher α transition temperature of the neat ABS. The prominent decrease in the storage modulus after the recovery peak results in more softening of the material and represents lower stress. For the neat ABS, the α transition starts at a high temperature of 86 °C (based on the DMTA curve). This phenomenon can cause a neglectable drop in the storage modulus and also a slight drop in the stress recovery plot for this structure. But for the other structures, due to the significant change in the storage modulus between the stress peak's temperature and 90 °C, the drops of stress in them are more obvious, causing a peak in stress recovery to be made, which is consistent with previous sources [38, 42]. These differences in actuation temperatures and stresses can provide us with a wide range of actuators for distinctive applications like grippers in soft robotics or pipe fasteners and splints in biomedical applications.

3.4. Adhesion

Figure 7 demonstrates the shear test results for each set of materials. As can be seen, the specimen that was made of the neat ABS shows the best shear strength, and its maximum shear stress is 21.70 MPa. Furthermore, there is a significant declining trend for

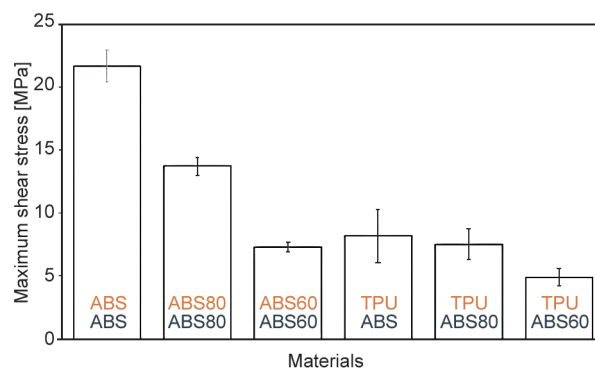


Figure 7. Maximum shear stress of each set of materials.

the maximum shear stress of the ABS80 and ABS60 specimens, which is associated with the softening of materials due to the incorporation of TPU in these composites. The maximum shear stresses are 13.70 and 7.30 MPa for ABS80 and ABS60 specimens, respectively. Also, there is a marginal descending trend for the maximum shear stress of bi-material structures. As it is depicted in Figure 7, the sample with the neat ABS and TPU has an 8.8 MPa maximum shear stress which is approximately 40% of the value associated with the ABS-ABS sample. These results have an excellent resemblance to Harris *et al.*'s [31] investigations of the maximum shear stress of ABS/ABS/ABS (15 MPa) and ABS/TPU/ABS (5 MPa). Based on the report of the comparison of the bi-material ABS-TPU structure with an industrial adhesive by Harris *et al.* [31], it can be deduced that the adhesion between the TPU and ABS is perfectly acceptable in this study. It is proof of the multi-material printability of these two materials for variant applications. Besides, the ABS80/TPU and ABS60/TPU structures manifest 7.2 and 4.5 MPa maximum shear stresses, which are about 50 and 60% of the values associated with relevant mono-material specimens, respectively. This ascending trend of these percentages could be related to the better adhesion of these composites to the TPU, which may be attributed to the presence of the dispersed TPU microdomains in the ABS matrix and the high affinity of the TPU layer to adhere to itself.

3.5. SEM

The interface of the TPU with the neat ABS and the composites printed layers is shown in Figure 8a–8c. As can be observed, there are excellent interfaces without any porosity and detachment between two materials in each image. Therefore, mechanical interlocking and filling all the voids and roughness of the

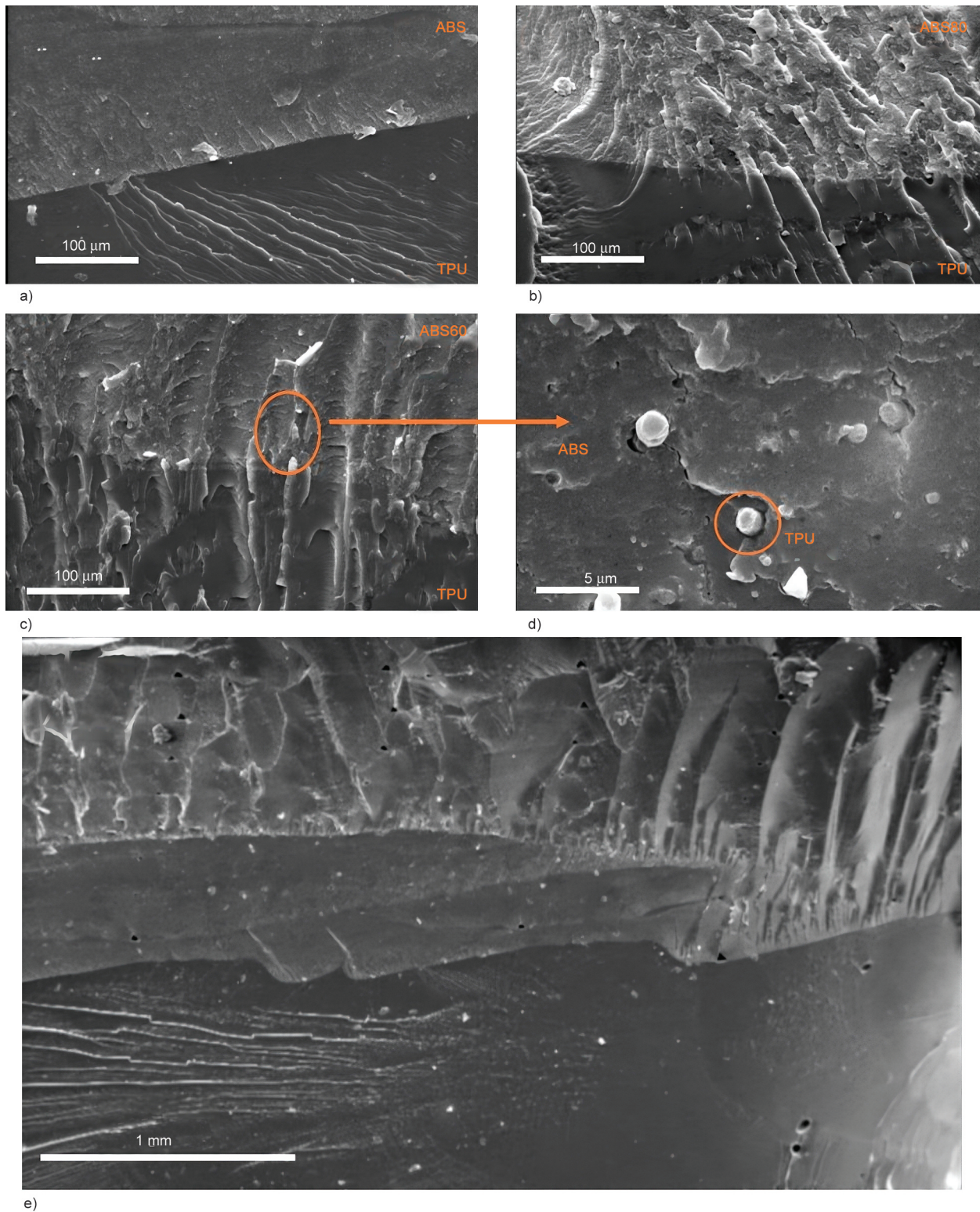


Figure 8. Scanning electron microscope of interface of a) ABS and TPU, b) ABS80 and TPU, c) ABS60 and TPU, d) morphology of the ABS60 composite; and e) bi-layer structure of the neat ABS and TPU.

thermoplastic layer's surface with the elastomeric material (TPU) is a promising approach for the good adhesion of the neat ABS and the blends with TPU. The reason for these phenomena is the low viscosity of the TPU at its printing temperature (220 °C). Also, as it was aforementioned, the TPU was printed on

the thermoplastics. Thus, during the printing procedure, high nozzle temperature (220 °C) and the hot extruded TPU may warm the surface of the thermoplastic up to even more than its glass transition temperature. Based on examinations of Yin *et al.* [32], the diffusion phenomenon can happen at the surface

of two polymers when the polymers reach above their glass transition temperatures. Concerning this matter, the TPU may have diffused into the neat ABS and the composites. In addition, Figure 8d shows the microscopic droplets of TPU in the ABS matrix. The average diameter of these droplets is 1 μm , which indicates the compatibility of the polyester-based TPU with the ABS [27]. Also, in Figure 8e, it can be seen that the bilayer specimens were printed in their best quality. Due to the low viscosity of TPU, the material was printed without any porosity. Furthermore, the thermoplastic layer has some neglectable voids between raster, but these voids don't deteriorate the shear stress results due to what was discussed above.

4. Conclusions

In this paper, a novel bi-layer macroscopic designed SMP structure was introduced using multi-material 4D printing and the basic microscopic concept of SMPs, hard and soft segments as network, and switching phases. The SME comes from the lamination assembly of stiff non-shape-memory thermoplastics like neat ABS, ABS80, and ABS60 composites and TPU elastomer TPU. Bi-layer ABS-TPU structures were 4D printed considering the thermoplastic and the thickness ratio of the constituent layers, and shape memory properties, thermal analysis, and microstructure were investigated. The below results were concluded.

- In the bi-layer structure, the thermoplastic is responsible for fixing the temporary shape in temperatures below its T_g by the rubber-to-glass hardening transition. During the programming steps, by cooling the deformed structure below the thermoplastic T_g , the elastic stress can be stored in the elastomer by the resistance of the stiffed glassy thermoplastic. When the structure is heated above the thermoplastic's T_g , the mentioned layer starts to soften, and the steep decrease in storage modulus leads to stored stress in the elastomer layer to be released.
- The highest shape fixity values (87.4 to 94.1%) were achieved for the ABS80. The reason for its superiority compared to pure ABS and ABS60 is the lower glass transition temperature and higher elastic modulus, respectively. On the other hand, ABS60 showed shape recovery ranges of 93% to 96.2% in the different thickness ratios of components, which is due to the more TPU phase.

The softening of the ABS80 and ABS60 composites at the deformation temperature caused the reduction of programming stress. The highest values of recovery ratio were obtained for ABS composites, which were 2.45 and 2.14 MPa for ABS80 and ABS60, respectively.

- Increasing the thickness ratio of the ABS layer caused more resistance against the release of the TPU layer in the programming step, and this trend was observed in all three bi-layer structures that, with the increase of ABS, fixity and recovery ratios increased and decreased, respectively.
- Neat ABS showed the best shear strength, and its maximum shear stress was 21.70 MPa. A significant declining trend for the maximum shear stress of the ABS composites was associated with the softening due to the incorporation of TPU in these composites. Besides, the ABS80/TPU and ABS60/TPU structures manifested 7.2 and 4.5 MPa maximum shear stresses, which were about 50 and 60% of the values associated with relevant mono-material specimens, respectively.
- The SEM results proved the excellent interfaces without any porosity and detachment between two ABS-TPU layers and mechanical interlocking, filling of all the voids and roughness of the thermoplastic layer's surface with the TPU was a promising approach for the good adhesion of the neat and ABS composites with TPU.

References

- [1] Soleyman E., Aberoumand M., Rahmatabadi D., Soltanmohammadi K., Ghasemi I., Baniassadi M., Abrinia K., Baghani M.: Assessment of controllable shape transformation, potential applications, and tensile shape memory properties of 3D printed PETG. *Journal of Materials Research and Technology*, **18**, 4201–4215 (2022).
<https://doi.org/10.1016/j.jmrt.2022.04.076>
- [2] Latif M., Jiang Y., Song J., Kim J.: Additively-manufactured high-concentration nanocellulose composites: Structure and mechanical properties. *Polymers*, **15**, 669 (2023).
<https://doi.org/10.3390/polym15030669>
- [3] Moradi M., Aminzadeh A., Rahmatabadi D., Rasouli S. A.: Statistical and experimental analysis of process parameters of 3D nylon printed parts by fused deposition modeling: Response surface modeling and optimization. *Journal of Materials Engineering and Performance*, **30**, 5441–5454 (2021).
<https://doi.org/10.1007/S11665-021-05848-4>

- [4] Rahmatabadi D., Soltanmohammadi K., Pahlavani M., Aberoumand M., Soleyman E., Ghasemi I., Baniassadi M., Abrinia K., Bodaghi M., Baghani M.: Shape memory performance assessment of FDM 3D printed PLA-TPU composites by Box-Behnken response surface methodology. *International Journal of Advanced Manufacturing Technology*, **127**, 935–950 (2023).
<https://doi.org/10.1007/s00170-023-11571-2>
- [5] Hassanien M., Alkhalder M., Abu-Nabah B. A., Abuzaid W.: A low-cost process for fabricating reinforced 3D printing thermoplastic filaments. *Polymers*, **15**, 315 (2023).
<https://doi.org/10.3390/polym15020315>
- [6] Rahmatabadi D., Soltanmohammadi K., Aberoumand M., Soleyman E., Ghasemi I., Baniassadi M., Abrinia K., Bodaghi M., Baghani M.: Development of pure poly (vinyl-chloride) (PVC) with excellent 3D printability and macro- and micro-structural properties. *Macromolecular Materials and Engineering*, **308**, 2200568 (2022).
<https://doi.org/10.1002/mame.202200568>
- [7] Leist S. K., Gao D., Chiou R., Zhou J.: Investigating the shape memory properties of 4D printed polylactic acid (PLA) and the concept of 4D printing onto nylon fabrics for the creation of smart textiles. *Virtual and Physical Prototyping*, **12**, 290–300 (2017).
<https://doi.org/10.1080/17452759.2017.1341815>
- [8] Vaezi M., Chianrabutra S., Mellor B., Yang S.: Multiple material additive manufacturing – Part 1: A review. *Virtual and Physical Prototyping*, **8**, 19–50 (2013).
<https://doi.org/10.1080/17452759.2013.778175>
- [9] Lumpe T. S., Mueller J., Shea K.: Tensile properties of multi-material interfaces in 3D printed parts. *Materials and Design*, **162**, 1–9 (2019).
<https://doi.org/10.1016/j.matdes.2018.11.024>
- [10] Tamburrino F., Graziosi S., Bordegoni M.: The influence of slicing parameters on the multi-material adhesion mechanisms of FDM printed parts: An exploratory study. *Virtual and Physical Prototyping*, **14**, 316–332 (2019).
<https://doi.org/10.1080/17452759.2019.1607758>
- [11] Li L., Liu W., Wang Y., Zhao Z.: Mechanical performance and damage monitoring of CFRP thermoplastic laminates with an open hole repaired by 3D printed patches. *Composite Structures*, **303**, 116308 (2023).
<https://doi.org/10.1016/j.compstruct.2022.116308>
- [12] Yang C., Wang B., Li D., Tian X.: Modelling and characterisation for the responsive performance of CF/PLA and CF/PEEK smart materials fabricated by 4D printing. *Virtual and Physical Prototyping*, **12**, 69–76 (2017).
<https://doi.org/10.1080/17452759.2016.1265992>
- [13] Gardan J.: Smart materials in additive manufacturing: State of the art and trends. *Virtual and Physical Prototyping*, **14**, 1–18 (2018).
<https://doi.org/10.1080/17452759.2018.1518016>
- [14] Yarali E., Baniassadi M., Zolfagharian A., Chavoshi M., Arefi F., Hossain M., Bastola A., Ansari M., Foyouzat A., Dabbagh A., Ebrahimi M., Mirzaali M. J., Bodaghi M.: Magneto-/ electro-responsive polymers toward manufacturing, characterization, and biomedical/ soft robotic applications. *Applied Materials Today*, **26**, 101306 (2022).
<https://doi.org/10.1016/j.apmt.2021.101306>
- [15] Leng J., Lan X., Liu Y., Du S.: Shape-memory polymers and their composites: Stimulus methods and applications. *Progress in Materials Science*, **56**, 1077–1135 (2011).
<https://doi.org/10.1016/j.pmatsci.2011.03.001>
- [16] Hager M. D., Bode S., Weber C., Schubert U. S.: Shape memory polymers: Past, present and future developments. *Progress in Polymer Science*, **49–50**, 3–33 (2015).
<https://doi.org/10.1016/j.progpolymsci.2015.04.002>
- [17] Soleyman E., Aberoumand M., Soltanmohammadi K., Rahmatabadi D., Ghasemi I., Baniassadi M., Abrinia K., Baghani M.: 4D printing of PET-G via FDM including tailor-made excess third shape. *Manufacturing Letters*, **33**, 1–4 (2022).
<https://doi.org/10.1016/j.mfglet.2022.05.002>
- [18] Xia L., Zhang M., Gao H., Qiu G., Xin Z., Fu W.: Thermal- and water-induced shape memory *Eucommia ulmoides* rubber and microcrystalline cellulose composites. *Polymer Testing*, **77**, 105910 (2019).
<https://doi.org/10.1016/j.polymertesting.2019.105910>
- [19] Melly S. K., Liu L., Liu Y., Leng J.: Active composites based on shape memory polymers: Overview, fabrication methods, applications, and future prospects. *Journal of Materials Science*, **55**, 10975–11051 (2020).
<https://doi.org/10.1007/s10853-020-04761-w>
- [20] Chen Y., Li J., Lu J., Ding M., Chen Y.: Synthesis and properties of poly(vinyl alcohol) hydrogels with high strength and toughness. *Polymer Testing*, **108**, 107516 (2022).
<https://doi.org/10.1016/j.polymertesting.2022.107516>
- [21] Xin X., Liu L., Liu Y., Leng J.: Mechanical models, structures, and applications of shape-memory polymers and their composites. *Acta Mechanica Solida Sinica*, **32**, 535–565 (2019).
<https://doi.org/10.1007/s10338-019-00103-9>
- [22] Meng H., Li G.: A review of stimuli-responsive shape memory polymer composites. *Polymer*, **54**, 2199–2221 (2013).
<https://doi.org/10.1016/j.polymer.2013.02.023>
- [23] Aberoumand M., Soltanmohammadi K., Rahmatabadi D., Soleyman E., Ghasemi I., Baniassadi M., Abrinia K., Bodaghi M., Baghani M.: 4D printing of poly(vinyl-chloride) (PVC): A detailed analysis of microstructure, programming, and shape memory performance. *Macromolecular Materials and Engineering*, **2023**, 2200677 (2023).
<https://doi.org/10.1002/MAME.202200677>

- [24] Wankhede V., Jagetiya D., Joshi A., Chaudhari R.: Experimental investigation of FDM process parameters using Taguchi analysis. *Materials Today: Proceedings*, **27**, 2117–2120 (2019).
<https://doi.org/10.1016/j.matpr.2019.09.078>
- [25] Rahmatabadi D., Ghasemi I., Baniassadi M., Abrinia K., Baghani M.: 4D printing of PLA-TPU blends: Effect of PLA concentration, loading mode, and programming temperature on the shape memory effect. *Journal of Materials Science*, **58**, 7227–7243 (2023).
<https://doi.org/10.1007/S10853-023-08460-0>
- [26] Huang X., Panahi-Sarmad M., Dong K., Cui Z., Zhang K., Gelis Gonzalez O., Xiao X.: 4D printed TPU/PLA/CNT wave structural composite with intelligent thermal-induced shape memory effect and synergistically enhanced mechanical properties. *Composites Part A: Applied Science and Manufacturing*, **158**, 106946 (2022).
<https://doi.org/10.1016/j.compositesa.2022.106946>
- [27] de León A. S., Domínguez-Calvo A., Molina S. I.: Materials with enhanced adhesive properties based on acrylonitrile-butadiene-styrene (ABS)/thermoplastic polyurethane (TPU) blends for fused filament fabrication (FFF). *Materials and Design*, **182**, 108044 (2019).
<https://doi.org/10.1016/j.matdes.2019.108044>
- [28] Packham D. E.: Surface energy, surface topography and adhesion. *International Journal of Adhesion and Adhesives*, **23**, 437–448 (2003).
[https://doi.org/10.1016/S0143-7496\(03\)00068-X](https://doi.org/10.1016/S0143-7496(03)00068-X)
- [29] Schultz J., Nardin M.: Theories and mechanisms of adhesion. in ‘Handbook of adhesive technology: Revised and expanded’ (eds.: Pizzi A., Mittal K. L.) CRC Press, Boca Raton, 3–18 (2017).
- [30] da Silva L. F. M., Öchsner A., Adams R. D.: *Handbook of adhesion technology*. Springer, Cham (2018).
<https://doi.org/10.1007/978-3-319-55411-2>
- [31] Harris C. G., Jursik N. J. S., Rochefort W. E., Walker T. W.: Additive manufacturing with soft TPU – Adhesion strength in multimaterial flexible joints. *Frontiers in Mechanical Engineering*, **5**, 37 (2019).
<https://doi.org/10.3389/fmech.2019.00037>
- [32] Yin J., Lu C., Fu J., Huang Y., Zheng Y.: Interfacial bonding during multi-material fused deposition modeling (FDM) process due to inter-molecular diffusion. *Materials and Design*, **150**, 104–112 (2018).
<https://doi.org/10.1016/j.matdes.2018.04.029>
- [33] Rahmatabadi D., Aberoumand M., Soltanmohammadi K., Soleyman E., Ghasemi I., Baniassadi M., Abrinia K., Bodaghi M., Baghani M.: Toughening PVC with biocompatible PCL softeners for supreme mechanical properties, morphology, shape memory effects, and FFF printability. *Macromolecular Materials and Engineering*, in press, 2300114 (2023).
<https://doi.org/10.1002/mame.202300114>
- [34] Siqueiros J. G., Schnittker K., Roberson D. A.: ABS-maleated SEBS blend as a 3D printable material. *Virtual and Physical Prototyping*, **11**, 123–131 (2016).
<https://doi.org/10.1080/17452759.2016.1175045>
- [35] Rocha C. R., Torrado Perez A. R., Roberson D. A., Shemelya C. M., Macdonald E., Wicker R. B.: Novel ABS-based binary and ternary polymer blends for material extrusion 3D printing. *Journal of Materials Research*, **29**, 1859–1866 (2014).
<https://doi.org/10.1557/JMR.2014.158>
- [36] Chávez A. F., Siqueiros J. G., Carrete I. A., Delgado I. L., Ritter G. W., Roberson D. A.: Characterisation of phases and deformation temperature for additively manufactured shape memory polymer components fabricated from rubberised acrylonitrile butadiene styrene. *Virtual and Physical Prototyping*, **14**, 188–202 (2018).
<https://doi.org/10.1080/17452759.2018.1550694>
- [37] Gnatowski A., Gołębski R., Sikora P.: Analysis of thermomechanical properties of polymeric materials produced by a 3D printing method. *Tehnički Glasnik*, **13**, 343–348 (2019).
<https://doi.org/10.31803/TG-20191102120738>
- [38] Soleyman E., Rahmatabadi D., Soltanmohammadi K., Aberoumand M., Ghasemi I., Abrinia K., Baniassadi M., Wang K., Baghani M.: Shape memory performance of PETG 4D printed parts under compression in cold, warm, and hot programming. *Smart Materials and Structures*, **31**, 085002 (2022).
<https://doi.org/10.1088/1361-665x/ac77cb>
- [39] Li G., Wang A.: Cold, warm, and hot programming of shape memory polymers. *Journal of Polymer Science Part B: Polymer Physics*, **54**, 1319–1339 (2016).
<https://doi.org/10.1002/polb.24041>
- [40] Du J., Armstrong S. R., Baer E.: Co-extruded multilayer shape memory materials: Comparing layered and blend architectures. *Polymer*, **54**, 5399–5407 (2013).
<https://doi.org/10.1016/j.polymer.2013.07.012>
- [41] Kim J-S., Lee D-Y., Koh J-S., Jung G-P., Cho K-J.: Component assembly with shape memory polymer fastener for microrobots. *Smart Materials and Structures*, **23**, 015011 (2013).
<https://doi.org/10.1088/0964-1726/23/1/015011>
- [42] Lim J. Y., Kim S. Y.: Thermal shrinkage stress in high-speed-spun, high molecular weight poly(ethylene terephthalate) filaments. *Journal of Polymer Science Part B: Polymer Physics*, **39**, 964–972 (2001).
<https://doi.org/10.1002/polb.1072>